



Published in final edited form as:

*J Biomed Mater Res A*. 2018 March ; 106(3): 663–672. doi:10.1002/jbm.a.36270.

## Three dimensional printed calcium phosphate and poly(caprolactone) composites with improved mechanical properties and preserved microstructure

Joseph B. Vella<sup>1,2,3</sup>, Ryan P. Trombetta<sup>1,2</sup>, Michael D. Hoffman<sup>1,2</sup>, Jason Inzana<sup>1,2</sup>, Hani Awad<sup>1,2</sup>, and Danielle S. W. Benoit<sup>1,2,4</sup>

<sup>1</sup>Department of Biomedical Engineering, University of Rochester, Rochester, New York 14627

<sup>2</sup>Center for Musculoskeletal Research, University of Rochester, Rochester, New York 14642

<sup>3</sup>Department of Otolaryngology, University of Rochester Medical Center, Rochester, New York 14642

<sup>4</sup>Department of Chemical Engineering, University of Rochester, Rochester, New York 14627

### Abstract

Biphase calcium phosphate scaffolds formed via three dimensional (3D) printing technology to exhibit porosity and chemical resorbability to promote osseointegration often lack the strength and toughness required to withstand loading in bone tissue engineering applications. Herein, sintering and CaP:poly(caprolactone) (PCL) composite formation were explored to improve 3D printed scaffold strength and toughness. Hydroxyapatite and  $\alpha$ -tricalcium phosphate ( $\alpha$ -TCP) biphase calcium powders were printed using phosphoric acid binder, which generated monetite and hydroxyapatite scaffolds. Upon sintering, evolution of  $\beta$ -TCP was observed along with an increase in flexural strength and modulus but no effect on fracture toughness was observed. Furthermore, scaffold porosity increased with sintering. Additionally, two techniques of PCL composite formation were employed: postprint precipitation and 3D print codeposition to further augment scaffold mechanical properties. While both techniques significantly improved flexural strength, flexural modulus, and fracture toughness under most conditions explored, precipitation yielded more substantial increases in these properties, which is attributed to better continuity of the PCL phase. However, precipitation also compromised surface porosity due to PCL passivation of the calcium phosphate surface, which may subsequently hinder scaffold integration and bone regeneration.

### Keywords

3D printing; calcium phosphate; mechanical property refinement; poly(caprolactone); ceramic composite

---

Correspondence to: D. S. W. Benoit; benoit@bme.rochester.edu.

Additional Supporting Information may be found in the online version of this article.

## INTRODUCTION

Over half a million bone grafts are required each year due to trauma, congenital malformations, and tumor resection.<sup>1-5</sup> The current gold standard for osseous reconstruction is autografts, which are accompanied by drawbacks that include greater surgical time and cost and increased risk of morbidity.<sup>6</sup> Alternatively, decellularized cadaveric allografts exhibit attractive mechanical stability as well as osteoconductive and osteoinductive properties.<sup>7,8</sup> However, allografts suffer poor host-graft integration and high prevalence of catastrophic failure (60% within 10 years),<sup>9,10</sup> which has motivated various regenerative strategies to augment healing.<sup>11-17</sup> However, allografts are further limited by difficulties in shaping to replicate the complex anatomical geometries necessary for successful graft-host integration.

Three-dimensional (3D) printing of ceramic biomaterials holds great promise for bone grafting. Ceramic scaffolds exhibit excellent biocompatibility and 3D printing allows faithful recapitulation of the geometry of native bone via preoperative computed tomography (CT) reconstructions of patient defect anatomy and computer aided design. Surgical applications of this approach include not only long bone reconstruction but also in craniomaxillofacial reconstruction where replication of more complex geometry promotes aesthetic outcomes and supports essential functions such as breathing, mastication, and speech.<sup>18,19</sup>

Numerous 3D printing technologies have been applied to create osteoconductive scaffolds for bone regeneration utilizing calcium phosphate materials, including material extrusion and binder jetting.<sup>20</sup> Material extrusion of ceramic slurries commonly employs a fluidized blend of a polymer and CaP particles typically requiring high temperatures for extrusion or subsequent sintering, which are not compatible with the incorporation of osteoinductive bioactive molecules to stimulate osteogenesis.<sup>21-23</sup> Alternatively, binder jetting enables low temperature bonding of CaP particles through the selective deposition of an aqueous binder (such as phosphoric acid) and is amenable to the incorporation of bioactives, which promote osteogenic cell mediated remodeling *in vivo*. The macro- and micromorphological characteristics of binder-jetted CaP scaffolds can be controlled by particle size selection, acid concentration, and postprinting processing, which can alter the mechanical properties and control the rate of chemical dissolution (resorption).<sup>22,24</sup> Therefore increasing efforts focused on developing low temperature printing techniques have shown important advances toward clinical translation.<sup>25,26</sup>

A primary challenge of ceramics remains the inferior mechanical properties for use in structural bone grafts. Although strength and toughness are typically inversely related,<sup>27</sup> bone possess an extraordinary combination of these two properties that has, thus far, not been emulated in man-made materials.<sup>28</sup> The unique properties of bone arise from the hierarchical organization of the collagen I and hydroxyapatite (HA) nanocomposite lamellae.<sup>28-34</sup> In contrast, CaP scaffolds lack the plastic deformability of bone.<sup>7,22,35-39</sup> Heat treatments<sup>26,40,41</sup> and formation of hybrid composites through polymer coatings applied post-printing or incorporation during fabrication<sup>42-46</sup> have been explored to increase CaP scaffold mechanical properties. However, adoption of these methods, including

comparisons of the two approaches, to enhance isotropic 3D printed CaP scaffolds, has not been reported.

Herein, two methods are explored to improve mechanical properties of 3D printed CaP scaffolds: sintering and incorporation of poly(caprolactone) (PCL) either during printing or as a postprinting/sintering coating. Specifically, 3D printed scaffolds of HA and  $\alpha$ -tricalcium phosphate ( $\alpha$ -TCP) powders were formed using established methods.<sup>38</sup> Then, as-printed and modified scaffolds were characterized with respect to crystallography, morphology, and mechanical properties to identify potential modifications that could enhance scaffold mechanical properties and enable use in load-bearing applications *in vivo*.

## MATERIALS AND METHODS

### Characterization of powders used in CaP scaffold fabrication

Particles of  $\alpha$ -TCP (30–70  $\mu\text{m}$  particle size, InnoTERE GmbH; Radebeul, Germany), HA (<70  $\mu\text{m}$ , InnoTERE), and PCL (14,000 g/mol, Sigma-Aldrich 440752, St. Louis, MO) used for scaffold fabrication were characterized using scanning electron microscopy (SEM) (Zeiss Auriga SEM/FIB Tool, Carl Zeiss Inc., Thornwood, NY). Particle size distributions were measured automatically using ImageJ (ImageJ, US National Institutes of Health, Bethesda, MA) using average axes measurements and elliptical particle size fitting (see Supporting Information Fig. S1 for examples of ImageJ processing).

### CaP scaffold fabrication and sintering

The powder printing process performed using a modified ZPrinter 450 (3D Systems; Andover, MA) is described in detail elsewhere.<sup>38</sup> Briefly, HA and  $\alpha$ -TCP powders in a 40:60 wt % composition were placed in a trough hopper, then spread evenly over the deposition stage with a roller. A 20 wt % (10.6 vol %) solution of phosphoric acid was then jetted over the powder layer through thermal inkjets (HP11, Hewlett-Packard; Palo Alto, CA), incurring a rapid sequential dissolution and reprecipitation of the  $\alpha$ -TCP phase. Of note, our previous work used a lower phosphoric acid concentration (8.75 wt % or 4.7 vol %) to preserve a codeposited collagen phase.<sup>38</sup> A higher concentration was used here to maximize the scaffold mechanical properties while preserving biocompatibility.<sup>47</sup> The powder layer thickness was set to 89  $\mu\text{m}$  and the binder liquid/powder ratio was set as 0.46 (homogeneous) in the ZPrint Software. This process was repeated to form rectangular blocks of  $1.5 \times 4.5 \times 10 \text{ mm}^3$  for three point flexural testing. All scaffolds were then postprocessed by flash dipping into an 0.1 wt % (0.053 vol %) phosphoric acid solution then washed repeatedly in deionized water to remove residual acid. Scaffolds were then sintered under atmospheric conditions in a tube furnace (21100 Tube Furnace, Barnstead Thermolyne Corp, Dubuque, IA) at 850 or 1000°C for 1 h or 1000°C for 6 h.

### CaP:PCL composite scaffold fabrication through codeposition or coating

PCL powder was codeposited with HA and  $\alpha$ -TCP powders by mixing in the powder trough at 1, 5, and 10 wt %. To create the powders, 5 wt % of PCL was dissolved in acetone at 60 °C with constant stirring for 20 min. PCL powder was then precipitated in deionized

water at room temperature. The powder was centrifuged and washed in deionized water three times and lyophilized for 24 h.

PCL coating of CaP scaffolds was achieved by immersion of printed scaffolds in solutions of 1, 5, or 10 wt % PCL in acetone at 60°C for 5 min. The scaffolds were then washed three times in deionized water and lyophilized for 24 h to remove residual water and acetone.

### Crystallographic and morphologic characterization of scaffolds

X-ray diffraction (XRD) was used to characterize the mineral phase that evolved following printing and sintering (Phillips X'Pert Multipurpose diffractometer, Phillips Corp, Westborough, MA). Average pore size, pore size distribution, and whole scaffold porosity was determined using microCT (VivaCT 40, Scanco Medical; Bassersdorf, Switzerland). Scaffold surface porosity, morphology, and polymer infiltration were characterized using SEM. Surface pore size distributions were automatically measured from thresholded images using ImageJ and elliptical particle size fitting based on the average axes of detected pores (see Fig. S1 for an example of ImageJ processing).

### Mechanical properties characterization

Three-point flexural testing was used to characterize the maximal flexural strength ( $\sigma_f$ ) and flexural modulus ( $E_f$ ), and fracture toughness ( $K_f$ ) using 10 mm loading fixtures (QTest5, MTS Systems Corp, Eden Prairie, MN). Fixed displacement rates (100  $\mu\text{m}/\text{min}$ ) were imposed on all samples over a test beam width of 10 mm. Mechanical properties ( $\sigma_f$ ,  $E_f$ ) were calculated according to ASTM D790 standards as follows:

$$\sigma_f = \frac{3FL}{2bd^2} \quad (1)$$

where  $F$  = maximum load (N),  $L$  = support span (10 mm),  $b$  = sample width (4.5 mm), and  $d$  = sample thickness (1.5 mm).

$$E_f = \frac{L^3 m}{4bd^3} \quad (2)$$

where  $m$  = slope of the initial linear portion of the load versus displacement curve (N/mm).

The fracture toughness ( $K_f$ ) was estimated by integrating the stress-strain curve as follows:

$$K_f = \int_0^{\varepsilon_f} \sigma_f d\varepsilon \quad (3)$$

where  $\varepsilon_f$  is strain at fracture. Three-point versus four-point bending testing was chosen due to limitations in specimen geometry to enable relative comparisons of strength between the different preparation methods. Additionally, three-point bending yields more conservative estimates of material properties, representing a worst-case loading condition, since brittle

ceramics are highly susceptible to shear and tension, which are both simultaneously induced in three-point bending at the same site (the load point) versus four-point testing.<sup>48,49</sup>

### Statistical analysis

All statistical comparisons were made in Prism (GraphPad) using Kruskal-Wallis nonparametric testing with Dunn's *post hoc* testing for pore size analysis and one-way analysis of variance (ANOVA) with Tukey's *post hoc* analysis for mechanical testing data. All data and error bars are represented as averages and standard deviations of at least four samples per condition, as detailed in figure legends. Differences were considered significant for  $p < 0.05$ .

## RESULTS

### Characterization of powders used in CaP scaffold fabrication

SEM imaging of  $\alpha$ -TCP, HA, and PCL powders used for 3D printing of CaP scaffolds was used for powder diameter and distribution analysis (Fig. 1).  $\alpha$ -TCP powder exhibited a polygonal morphology with an average diameter of  $56 \pm 27 \mu\text{m}$  whereas HA showed spherical particle morphology with an average diameter of  $27 \pm 10 \mu\text{m}$ . PCL used for codeposition showed a polygonal morphology with an average particle diameter of  $256 \pm 100 \mu\text{m}$ .

### CaP phase evolution of printed and sintered bone scaffolds

XRD was used to investigate the CaP phases present in green as-printed and sintered scaffolds (Fig. 2). During the 3D printing process, the acid binder reacted exclusively with the  $\alpha$ -TCP phase to form a monetite phase. This can be seen by conservation of the HA peaks in the as-printed scaffold [Fig. 2(c)] with the loss of characteristic peaks of  $\alpha$ -TCP. The phase that was precipitated at the expense of the  $\alpha$ -TCP was shown to be the dicalcium phosphate or monetite. However, upon sintering, all phases (HA,  $\alpha$ -TCP, and monetite) are consumed and substantial growth of  $\beta$ -TCP phase was observed [Fig. 2(d)]. These trends are also supported by exploded views of characteristic diffraction peaks of the four phases that evolve from these processes in Figure 3.

### Porosity and morphologic characterization of scaffolds

Scaffold surface morphology and porosity were characterized using SEM, as shown in Figure 4. Qualitatively, only subtle changes in surface morphology were observed between the as-printed scaffolds and the sintered scaffolds, mainly reflecting crystal morphology and the evolution of  $\beta$ -TCP phase. PCL precipitation onto as-printed scaffolds decreased surface roughness with increasing PCL solution concentration (1, 5, and 10 wt %) as the PCL coated the underlying scaffold mineral phase. While 1 wt % showed decreased surface roughness and partial coverage of the calcium phosphate particles, precipitation of 5 wt % PCL further reduced surface roughness and increased coating of the scaffold calcium phosphate. Precipitation of 10 wt % PCL completely effaced scaffold surface roughness due PCL coating the underlying scaffold. Conversely, sintered scaffolds with codeposited PCL showed no effects of increasing PCL concentration from 1 to 5% on the surface roughness and coating of the mineral particles. Upon quantification of porosity using ImageJ, no

statistically significant differences in mean surface porosities were observed for any of the scaffolds analyzed.

Quantitatively, pore size significantly increased due to sintering versus as-printed scaffolds from  $8.3 \pm 8.4$  to  $9.9 \pm 9.8$   $\mu\text{m}$ . PCL precipitation yielded pore sizes of  $9.4 \pm 9.8$ ,  $7.1 \pm 6.0$ , and  $9.7 \pm 10.3$   $\mu\text{m}$  for 1, 5, and 10%. The effect of PCL precipitation on pore size is not concentration dependent where 5 wt % exhibits decreased size versus 1 wt % but neither 5 nor 1 wt % pore size is different from 10 wt %. In fact, when comparing within the same PCL modification approach, only 1 and 5% PCL precipitation yielded significantly different pore sizes of  $9.4 \pm 9.8$  and  $7.1 \pm 6.0$   $\mu\text{m}$ . Scaffolds formed through codeposition overall exhibited lower pore sizes versus the PCL precipitated scaffolds. Codeposition of PCL at 1 wt % resulted in average pore sizes of  $7.2 \pm 6.1$   $\mu\text{m}$ , which is statistically similar to both as-printed and 5 wt % codeposited scaffolds (pore size of  $6.8 \pm 6.0$   $\mu\text{m}$ ) (see Supplemental Table 1 for all *p*-values from analyses).

### Mechanical properties characterization

The mechanical properties of the 3D printed CaP scaffolds were analyzed through three-point bending and data are summarized in Figure 5. Sintering at 1000°C for 1 or 6 h resulted in significant increases of 80% in flexural strength and 50–100% in modulus compared to as-printed scaffolds, while 850°C sintered only significantly improved modulus by 40% over as-printed scaffolds. However, no significant increases in fracture toughness were attained by sintering. PCL precipitated scaffolds at all conditions showed dramatic increases in scaffold strength, modulus, and fracture toughness. Specifically, at 1 wt % PCL flexural strength and modulus increased ~100% compared to as-printed scaffolds while fracture toughness increased 180%. Interestingly, increasing from 1 to 10 wt % in the PCL precipitated solution only modestly increased fracture toughness from 11 to 14.5 kJ/m<sup>3</sup>. No other properties exhibited significant differences in mechanical properties due to increasing PCL wt %. PCL codeposition also significantly increased mechanical properties compared to unsintered CaP scaffolds, albeit to a lesser extent than PCL precipitation, with 90 and 55% increases in flexural strength, 65 and 45% increases in modulus, but no significant changes in toughness for 1 and 5 wt % PCL co-deposition were found compared to unsintered CaP.

## DISCUSSION

For successful bone scaffold development, it is critical for materials to exhibit mechanical properties, morphology, and structure to allow for load bearing, degradation, bone ingrowth, and remodeling. Though CaP materials are commonly used for bone scaffolds, and some are approved by the food and drug administration (FDA) as bone void fillers, their material properties continue to fall short of required functional criteria. Though with the recent development of 3D printing techniques, complex geometries of isotropic materials are attainable and porosity is more readily controlled, poor mechanical properties, in particular brittle behavior, continue to be a significant limitation. Here, two approaches were examined that enhance the mechanical properties yet maintain porosity and morphology of 3D printed CaP scaffold fabrication. The two methods involved heat treatment (sintering) and

incorporation of polymer (PCL) through codeposition during printing or through post-printing precipitation. Both methods resulted in significant improvements in scaffold flexural strength and modulus, and, for polymer incorporation, fracture toughness.

Scaffold degradation and mechanical properties are governed by scaffold structure as well as ceramic phases, which was investigated herein. In particular, the green as-printed scaffold, which is primarily comprised of monetite and HA, exhibited flexural strength on the low end of cancellous bone.<sup>50,51</sup> Sintering, which has been reported to strengthen CaP up to fourfold through phase transitions to  $\beta$ -TCP,<sup>37,39</sup> increased modulus here by up to 100%, but this value was still within the range of cancellous bone. These findings are consistent with recent reports, which show increases in CaP scaffold strength with rising  $\beta$ -TCP content.<sup>35,36</sup> Interestingly, sintering does little to affect fracture toughness of CaP scaffolds tested here despite previous reports suggesting sintering alters pore morphology and grain boundaries.<sup>26,40,41</sup> This may be due to stark differences in original grain structure of 3D printed versus bulk CaP or sintering conditions, in particular, higher temperatures and longer sintering times employed elsewhere.<sup>26,40,41</sup>

CaP scaffolds formed through 3D printing have been achieved using various phases and methods.<sup>24</sup> Chemical evolution of HA, which mimics the inorganic mineral matrix of bone, into 3D printed scaffolds requires strong acids for dissolution which may elute *in vivo* or may preclude bioactive molecule incorporation during printing. Therefore, more soluble calcium phosphate phases in weaker acids have been employed, such as  $\alpha$ -TCP, which undergoes a phase transition to monetite and forms the “glue” to bind nondissolved HA particles, as employed here and in our previous work.<sup>38</sup> Under these conditions, which avoids use of high temperatures common to indirect rapid prototyping (negative molding) techniques yet result in similar scaffold mechanics,<sup>52,53</sup> bioactive, temperature-sensitive drugs and extracellular matrix (ECM) cues, such as collagen, have been codeposited, resulting in osteogenic remodeling.<sup>38</sup> Interestingly, the phosphoric acid-based binding of  $\alpha$ -TCP/HA realizes a composite phase of HA and monetite. Though brushite versus monetite typically results from the dissolution reprecipitation reaction of CaP and phosphoric acid,<sup>24,38,54–56</sup> crystallization conditions, including humidity and acidic pH bias to the more stable but typically kinetically hindered monetite phase, which is observed here.<sup>57–59</sup> Upon implantation, the HA phase of the composite is nondegradable, resulting in graft “inclusion” rather than “substitution.”<sup>54,55</sup> To increase degradability at the expense of structural and functional preservation of biological cues, sintering can be used to convert the mineral phase to  $\beta$ -TCP, which increases the rate of CaP degradation to match bone ingrowth.<sup>60–63</sup> Thus, there are significant opportunities to ensure biologically active, degradable CaP scaffold development, including use of other compositional phases, such as octacalcium phosphates, which have recently gained favor for their enhanced biological properties.<sup>64–67</sup>

Introduction of binding agents, such as polymers, can further enhance CaP scaffold mechanics. For example, polymers such as poly(lactic acid) (PLA) and poly(glycolic acid) (PGA) or poly(lactide-co-glycolide) (PLGA) copolymers have been incorporated to enhance scaffold mechanical properties. Depending upon polymer properties and method of incorporation, polymers have been shown to increase compressive modulus of HA-based scaffolds up to 11-fold.<sup>26,42–44,46,56,68</sup> Here, we showed incorporation of PCL via

precipitation postprinting or through codeposition during printing dramatically improved scaffold strength and modulus up to 2.6-fold compared to as-printed scaffolds. However, the most dramatic improvements were shown in scaffold toughness with an almost fourfold increase for PCL precipitated scaffolds formed here, which outperformed codeposited PCL toughness by approximately twofold. This dramatic increase in toughness has been previously reported for CaP scaffolds modified through PLGA precipitation, which yielded fourfold greater modulus and greater than eightfold higher scaffold toughness.<sup>26,45</sup> Toughness greatly depends on scaffold microporosity, including pore size and morphology. The pore characteristics reduce crack propagation in materials, as the pores redistribute released energy during mechanical force input.<sup>45,69–71</sup> Pore sizes obtained using SEM from PCL-precipitated scaffolds support this finding as they were statistically lower than those of as-printed scaffolds. Polymer coatings have been posited to increase both compressive strength and toughness due to a combination of crack bridging and coating of scaffold struts as the polymer acts as a glue the ceramic structure, reducing brittleness and increasing toughness during mechanical testing.<sup>45</sup> Interestingly, PCL precipitation yields approximately twofold greater toughness compared to codeposition. Codeposited PCL is exposed to acid briefly during the printing process to achieve polymer diffusion/integration. Therefore, the PCL phase is unlikely to adopt the continuous glue phase achieved by the dissolved-then-precipitated PCL, albeit with limited scaffold infiltration, that results in superior scaffold toughness. Codeposition of PCL or similar polymers followed by heating to near or above the polymer melting temperature may achieve polymer continuity within CaP scaffolds to further improve mechanical properties. However, as PCL content and continuity increases, CaP scaffold porosity is likely to become obscured, limiting scaffold osseointegration and remodeling.

Despite dramatic increases in scaffold mechanical properties through postprint coating of PCL, there are some drawbacks to this approach. Infiltration of the polymer was limited to approximately 200–300  $\mu\text{m}$ , similar to previous studies,<sup>26,46</sup> resulting in superficial polymer incorporation, which limits wide applicability of this approach in human sized scaffolds. For example, scaffolds with small surface area to volume ratios, overall increases in mechanical properties would be far less than tested here due to poor infiltration of the polymer. Alternatively, vacuum-assisted polymer coating of the scaffold may improve penetration depths, resulting in increased mechanical properties of various CaP-based scaffolds.<sup>45,72</sup> In one study, compressive strength increased from 0.07 to 5.44 MPa following vacuum-assisted coating of CaP scaffolds.<sup>72</sup> Furthermore, for PCL precipitation, which had the greatest impact on mechanical properties, as PCL concentration increases, CaP surface exposure is reduced. In fact, at 10% PCL precipitation, CaP appears to be completely coated with the polymer, which may alter cell–material interactions and biocompatibility of the scaffold. Furthermore, PLGA coatings and the associated acidic degradation products can result in the foreign body reaction or inflammatory responses.<sup>73,74</sup> However, as it provides more favorable conditions for osteogenic cells,<sup>46</sup> PCL may circumvent these challenges, although cell interactions are not explicitly studied here.

## CONCLUSION

Sintering and incorporation of PCL were investigated to improve 3D printed CaP scaffold mechanical properties. Though sintering improved scaffold flexural strength and modulus, likely through conversion of the composite HA/monetite to  $\beta$ -TCP, fracture toughness was not enhanced. Alternatively, PCL was incorporated either postprinting using a precipitation coating method or during printing using codeposition with HA/ $\alpha$ -TCP powders. Both of these approaches resulted in dramatic increases in scaffold flexural strength, modulus, and fracture toughness, especially when using increased concentrations of precipitated PCL. Despite these improvements, the CaP scaffold surface is completely covered by PCL at conditions that result in the greatest mechanical properties, which is likely to impact tissue integration and subsequent graft remodeling and overall healing. Nonetheless, this investigation illustrates scaffold modification techniques to improve properties for subsequent use in bone tissue engineering applications.

## Supplementary Material

Refer to Web version on PubMed Central for supplementary material.

## Acknowledgments

Contract grant sponsor: NIH; contract grant numbers: R01AR064200, P30AR069655

Contract grant sponsor: American Academy of Facial Plastic and Reconstructive Surgery (AAFPRS) Leslie Bernstein Resident Research Grant; contract grant number: 352604

The authors would like to thank Mike Thullen and Chris Pratt for their technical assistance and the Center for Musculoskeletal Research for use of their facilities.

## References

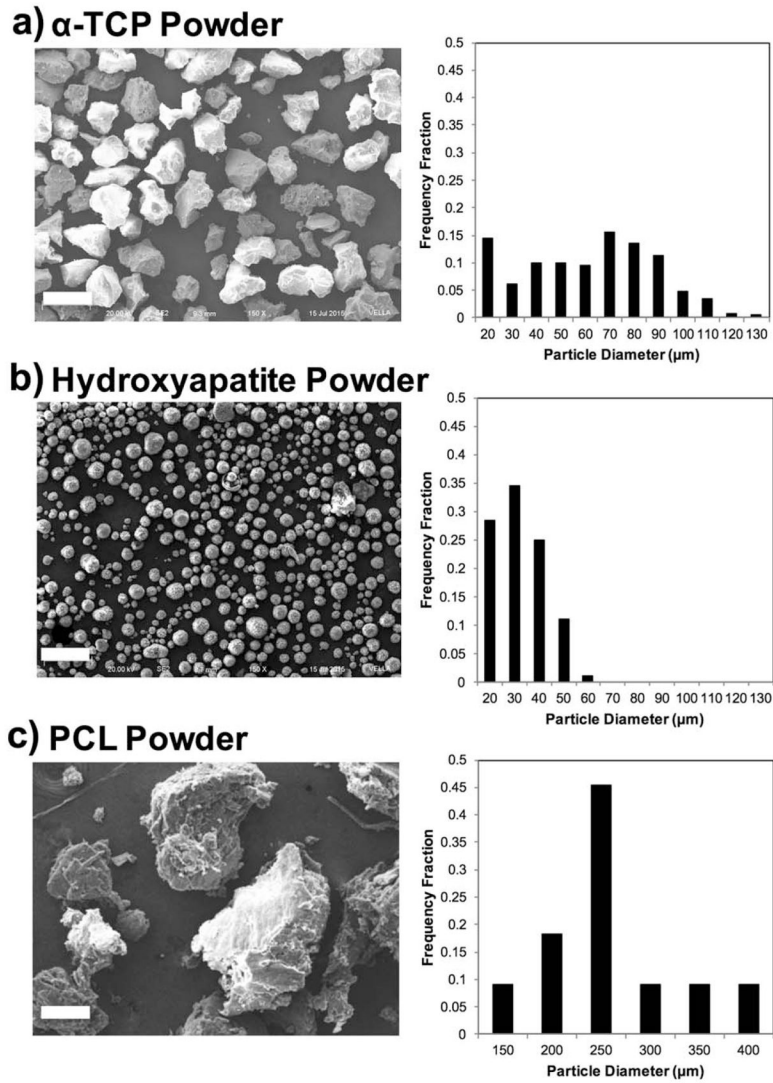
1. Kellman RM, Tatum SA. Pediatric craniomaxillofacial trauma. *Facial Plast Surg Clin North Am.* 2014; 22:559–572. [PubMed: 25444728]
2. Lee LN, Bhattacharyya N. Contemporary trends in procedural volume for adult facial trauma, 1996–2006. *Otolaryngol Head Neck Surg.* 2012; 146:226–229. [PubMed: 22063732]
3. Hayden RE, Nagel TH. The evolving role of free flaps and pedicled flaps in head and neck reconstruction. *Curr Opin Otolaryngol Head Neck Surg.* 2013; 21:305–310. [PubMed: 23842288]
4. Gentile MA, Tellington AJ, Burke WJ, Jaskolka MS. Management of midface maxillofacial trauma. *Atlas Oral Maxillofac Surg Clin.* 2013; 21:69–95.
5. Zamiri B, Shahidi S, Eslaminejad MB, Khoshzaban A, Gholami M, Bahramnejad E, Moghadasali R, Mardpour S, Aghdami N. Reconstruction of human mandibular continuity defects with allogenic scaffold and autologous marrow mesenchymal stem cells. *J Craniofac Surg.* 2013; 24:1292–1297. [PubMed: 23851791]
6. Tarafder S, Davies NM, Bandyopadhyay A, Bose S. 3D printed tri-calcium phosphate bone tissue engineering scaffolds: Effect of SrO and MgO doping on in vivo osteogenesis in a rat distal femoral defect model. *Biomater Sci.* 2013; 1:1250–1259. [PubMed: 24729867]
7. Karageorgiou V, Kaplan D. Porosity of 3D biomaterial scaffolds and osteogenesis. *Biomaterials.* 2005; 26:5474–5491. [PubMed: 15860204]
8. Chatterjea A, van der Stok J, Danoux CB, Yuan HP, Habibovic P, van Blitterswijk CA, Weinans H, de Boer J. Inflammatory response and bone healing capacity of two porous calcium phosphate ceramics in critical size cortical bone defects. *J Biomed Mater Res Part A.* 2014; 102:1399–1407.

9. Mankin HJ, Gebhardt MC, Jennings LC, Springfield DS, Tomford WW. Long-term results of allograft replacement in the management of bone tumors. *Clin Orthop Relat Res.* 1996; 324:86–97.
10. Muscolo DL, Ayerza MA, Aponte-Tinao LA. Long-term results of allograft replacement after total calcanectomy. A report of two cases. *J Bone Joint Surg Am.* 2000; 82:109–112. [PubMed: 10653091]
11. Hoffman MD, Benoit DS. Emulating native periosteum cell population and subsequent paracrine factor production to promote tissue engineered periosteum-mediated allograft healing. *Biomaterials.* 2015; 52:426–440. [PubMed: 25818449]
12. Hoffman MD, Benoit DS. Emerging ideas: Engineering the periosteum: Revitalizing allografts by mimicking autograft healing. *Clin Orthop Relat Res.* 2013; 471:721–726. [PubMed: 23179118]
13. Hoffman MD, Van Hove AH, Benoit DS. Degradable hydrogels for spatiotemporal control of mesenchymal stem cells localized at decellularized bone allografts. *Acta Biomater.* 2014; 10:3431–3441. [PubMed: 24751534]
14. Hoffman MD, Xie C, Zhang X, Benoit DS. The effect of mesenchymal stem cells delivered via hydrogel-based tissue engineered periosteum on bone allograft healing. *Biomaterials.* 2013; 34:8887–8898. [PubMed: 23958029]
15. Van Hove AH, Antonienko E, Burke K, Brown E 3rd, Benoit DS. Temporally tunable, enzymatically responsive delivery of proangiogenic peptides from poly(ethylene glycol) hydrogels. *Adv Healthc Mater.* 2015; 4:2002–2011. [PubMed: 26149620]
16. Van Hove AH, Benoit DS. Depot-based delivery systems for proangiogenic peptides: A review. *Front Bioeng Biotechnol.* 2015; 3:102. [PubMed: 26236708]
17. Van Hove AH, Burke K, Antonienko E, Brown E 3rd, Benoit DS. Enzymatically-responsive proangiogenic peptide-releasing poly(-ethylene glycol) hydrogels promote vascularization in vivo. *J Control Release.* 2015; 217:191–201. [PubMed: 26365781]
18. Futran ND, Mendez E. Developments in reconstruction of midface and maxilla. *Lancet Oncol.* 2006; 7:249–258. [PubMed: 16510334]
19. Tamimi F, Torres J, Gbureck U, Lopez-Cabarcos E, Bassett DC, Alkhraisat MH, Barralet JE. Craniofacial vertical bone augmentation: A comparison between 3D printed monolithic monetite blocks and autologous onlay grafts in the rabbit. *Biomaterials.* 2009; 30:6318–6326. [PubMed: 19695698]
20. Habibovic P, Gbureck U, Doillon CJ, Bassett DC, van Blitterswijk CA, Barralet JE. Osteoconduction and osteoinduction of low-temperature 3D printed bioceramic implants. *Biomaterials.* 2008; 29:944–953. [PubMed: 18055009]
21. Fierz FC, Beckmann F, Huser M, Irsen SH, Leukers B, Witte F, Degistirici Ö, Andronache A, Thie M, Müller B. The morphology of anisotropic 3D-printed hydroxyapatite scaffolds. *Biomaterials.* 2008; 29:3799–3806. [PubMed: 18606446]
22. Chumnanklang R, Panyathanmaporn T, Sitthiseripratip K, Suwanprateeb J. 3D printing of hydroxyapatite: Effect of binder concentration in pre-coated particle on part strength. *Mater Sci Eng C.* 2007; 27:914–921.
23. Gbureck U, Vorndran E, Müller FA, Barralet JE. Low temperature direct 3D printed bioceramics and biocomposites as drug release matrices. *J Control Release.* 2007; 122:173–180. [PubMed: 17655962]
24. Trombetta R, Inzana JA, Schwarz EM, Kates SL, Awad HA. 3D printing of calcium phosphate ceramics for bone tissue engineering and drug delivery. *Ann Biomed Eng.* 2017; 45:23–44. [PubMed: 27324800]
25. Hannink G, Arts JJC. Bioresorbability, porosity and mechanical strength of bone substitutes: What is optimal for bone regeneration? *Injury.* 2011; 42:S22–S25.
26. Miguel C, Claus M, Andrea E, Uwe G, Jürgen G, Inês P, Jörg T, Elke V. Direct 3D powder printing of biphasic calcium phosphate scaffolds for substitution of complex bone defects. *Biofabrication.* 2014; 6:015006. [PubMed: 24429776]
27. Ritchie RO. The conflicts between strength and toughness. *Nat Mater.* 2011; 10:817–822. [PubMed: 22020005]
28. Chen PY, McKittrick J, Meyers MA. Biological materials: Functional adaptations and bioinspired designs. *Prog Mater Sci.* 2012; 57:1492–1704.

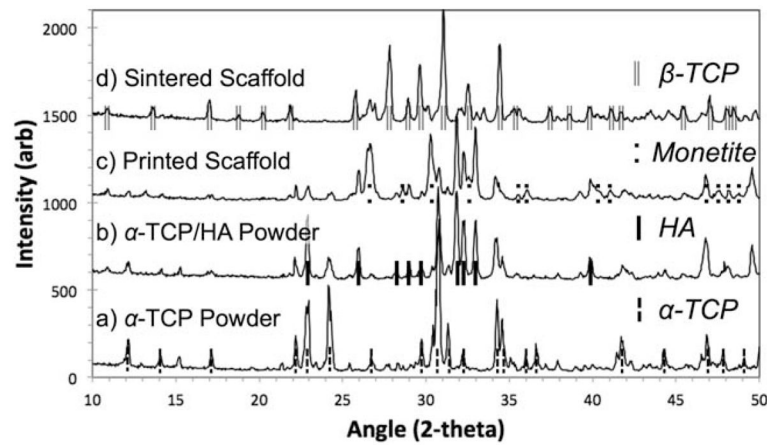
29. Currey JD. Materials science. Hierarchies in biomineral structures. *Science*. 2005; 309:253–254. [PubMed: 16002605]
30. Fantner GE, Hassenkam T, Kindt JH, Weaver JC, Birkedal H, Pechenik L, Cutroni JA, Cidade GAG, Stucky GD, Morse DE, Hansma PK. Sacrificial bonds and hidden length dissipate energy as mineralized fibrils separate during bone fracture. *Nat Mater*. 2005; 4:612–616. [PubMed: 16025123]
31. Gao H, Ji B, Jager IL, Arzt E, Fratzl P. Materials become insensitive to flaws at nanoscale: Lessons from nature. *Proc Natl Acad Sci USA*. 2003; 100:5597–5600. [PubMed: 12732735]
32. Meyers MA, McKittrick J, Chen PY. Structural biological materials: Critical mechanics-materials connections. *Science*. 2013; 339:773–779. [PubMed: 23413348]
33. Pasteris JD, Wopenka B, Freeman JJ, Rogers K, Valsami-Jones E, van der Houwen JA, Silva MJ. Lack of OH in nanocrystalline apatite as a function of degree of atomic order: Implications for bone and biomaterials. *Biomaterials*. 2004; 25:229–238. [PubMed: 14585710]
34. Tertuliano OA, Greer JR. The nanocomposite nature of bone drives its strength and damage resistance. *Nat Mater*. 2016; 15:1195–1202. [PubMed: 27500809]
35. Metsger DS, Rieger MR, Foreman DW. Mechanical properties of sintered hydroxyapatite and tricalcium phosphate ceramic. *J Mater Sci Mater Med*. 1999; 10:9–17. [PubMed: 15347989]
36. Zyman ZZ, Tkachenko MV, Polevodin DV. Preparation and characterization of biphasic calcium phosphate ceramics of desired composition. *J Mater Sci Mater Med*. 2008; 19:2819–2825. [PubMed: 18322781]
37. Bergmann C, Lindner M, Zhang W, Koczur K, Kirsten A, Telle R, Fischer H. 3D printing of bone substitute implants using calcium phosphate and bioactive glasses. *J Eur Ceram Soc*. 2010; 30:2563–2567.
38. Inzana JA, Olvera D, Fuller SM, Kelly JP, Graeve OA, Schwarz EM, Kates SL, Awad HA. 3D printing of composite calcium phosphate and collagen scaffolds for bone regeneration. *Biomaterials*. 2014; 35:4026–4034. [PubMed: 24529628]
39. Lowmunkong R, Sohmura T, Suzuki Y, Matsuya S, Ishikawa K. Fabrication of freeform bone-filling calcium phosphate ceramics by gypsum 3D printing method. *J Biomed Mater Res B*. 2009; 90B:531–539.
40. Bose S, Dasgupta S, Tarafder S, Bandyopadhyay A. Microwave-processed nanocrystalline hydroxyapatite: Simultaneous enhancement of mechanical and biological properties. *Acta Biomater*. 2010; 6:3782–3790. [PubMed: 20230922]
41. Veljovic DJ, Palcevskis E, Dindune A, Putic S, Balac I, Petrovic R, Janackovic DD. Microwave sintering improves the mechanical properties of biphasic calcium phosphates from hydroxyapatite microspheres produced from hydrothermal processing. *J Mater Sci*. 2010; 45:3175–3183.
42. Qi X, Ye J, Wang Y. Alginate/poly(lactic-co-glycolic acid)/calcium phosphate cement scaffold with oriented pore structure for bone tissue engineering. *J Biomed Mater Res A*. 2009; 89:980–987. [PubMed: 18470921]
43. Zhang R, Ma PX. Porous poly(L-lactic acid)/apatite composites created by biomimetic process. *J Biomed Mater Res*. 1999; 45:285–293. [PubMed: 10321700]
44. Zhao J, Lu X, Duan K, Guo LY, Zhou SB, Weng J. Improving mechanical and biological properties of macroporous HA scaffolds through composite coatings. *Colloids Surf B*. 2009; 74:159–166.
45. Kang Y, Scully A, Young DA, Kim S, Tsao H, Sen M, Yang Y. Enhanced mechanical performance and biological evaluation of a PLGA coated beta-TCP composite scaffold for load-bearing applications. *Eur Polym J*. 2011; 47:1569–1577. [PubMed: 21892228]
46. Peroglio M, Gremillard L, Gauthier C, Chazeau L, Verrier S, Alini M, Chevalier J. Mechanical properties and cytocompatibility of poly(epsilon-caprolactone)-infiltrated biphasic calcium phosphate scaffolds with bimodal pore distribution. *Acta Biomater*. 2010; 6:4369–4379. [PubMed: 20553981]
47. Gbureck U, Hölzel T, Doillon CJ, Müller FA, Barralet JE. Direct printing of bioceramic implants with spatially localized angiogenic factors. *Adv Mater*. 2007; 19:795–800.
48. Mujika F. On the difference between flexural moduli obtained by three-point and four-point bending tests. *Polym Test*. 2006; 25:214–220.

49. Quinn GD, Sparenberg BT, Koshy P, Ives LK, Jahanmir S, Arola DD. Flexural strength of ceramic and glass rods. *J Test Eval*. 2009; 37:222–244.
50. Carter DR, Hayes WC. The compressive behavior of bone as a two-phase porous structure. *J Bone Joint Surg Am*. 1977; 59:954–962. [PubMed: 561786]
51. Hing KA. Bone repair in the twenty-first century: Biology, chemistry or engineering? *Philos Trans A Math Phys Eng Sci*. 2004; 362:2821–2850. [PubMed: 15539372]
52. Schumacher M, Deisinger U, Detsch R, Ziegler G. Indirect rapid prototyping of biphasic calcium phosphate scaffolds as bone substitutes: Influence of phase composition, macroporosity and pore geometry on mechanical properties. *J Mater Sci Mater Med*. 2010; 21:3119–3127. [PubMed: 20953674]
53. Schumacher M, Uhl F, Detsch R, Deisinger U, Ziegler G. Static and dynamic cultivation of bone marrow stromal cells on biphasic calcium phosphate scaffolds derived from an indirect rapid prototyping technique. *J Mater Sci Mater Med*. 2010; 21:3039–3048. [PubMed: 20857322]
54. Klammert U, Gbureck U, Vorndran E, Rödiger J, Meyer-Marcotty P, Kübler AC. 3D powder printed calcium phosphate implants for reconstruction of cranial and maxillofacial defects. *J Craniomaxillofac Surg*. 2010; 38:565–570. [PubMed: 20206538]
55. Lobo SE, Arinze LT. Biphasic calcium phosphate ceramics for bone regeneration and tissue engineering applications. *Materials*. 2010; 3:815–826.
56. Seitz H, Rieder W, Irsen S, Leukers B, Tille C. Three-dimensional printing of porous ceramic scaffolds for bone tissue engineering. *J Biomed Mater Res B Appl Biomater*. 2005; 74:782–788. [PubMed: 15981173]
57. Bohner M, Merkle HP, Lemaître J. In vitro aging of a calcium phosphate cement. *J Mater Sci Mater Med*. 2000; 11:155–162. [PubMed: 15348044]
58. Bohner M, Van Landuyt P, Merkle HP, Lemaître J. Composition effects on the pH of a hydraulic calcium phosphate cement. *J Mater Sci Mater Med*. 1997; 8:675–681. [PubMed: 15348818]
59. Mirtchi AA, Lemaître J, Terao N. Calcium phosphate cements: Study of the beta-tricalcium phosphate–monocalcium phosphate system. *Biomaterials*. 1989; 10:475–480. [PubMed: 2804235]
60. Arinze TL, Tran T, McAlary J, Daculsi G. A comparative study of biphasic calcium phosphate ceramics for human mesenchymal stem-cell-induced bone formation. *Biomaterials*. 2005; 26:3631–3638. [PubMed: 15621253]
61. Benahmed M, Bouler JM, Heymann D, Gan O, Daculsi G. Biodegradation of synthetic biphasic calcium phosphate by human monocytes in vitro: A morphological study. *Biomaterials*. 1996; 17:2173–2178. [PubMed: 8922603]
62. Gauthier O, Bouler JM, Aguado E, Pilet P, Daculsi G. Macroporous biphasic calcium phosphate ceramics: Influence of macropore diameter and macroporosity percentage on bone ingrowth. *Biomaterials*. 1998; 19:133–139. [PubMed: 9678860]
63. Nery EB, LeGeros RZ, Lynch KL, Lee K. Tissue response to biphasic calcium phosphate ceramic with different ratios of HA/beta TCP in periodontal osseous defects. *J Periodontol*. 1992; 63:729–735. [PubMed: 1335498]
64. Komlev VS, Barinov SM, Bozo II, Deev RV, Eremin II, Fedotov AY, Gurin AN, Khromova NV, Kopnin PB, Kuvshinova EA, Mamonov VE, Rybko VA, Sergeeva NS, Teterina AY, Zorin VL. Bioceramics composed of octacalcium phosphate demonstrate enhanced biological behavior. *ACS Appl Mater Interfaces*. 2014; 6:16610–16620. [PubMed: 25184694]
65. Liu Y, Cooper PR, Barralet JE, Shelton RM. Influence of calcium phosphate crystal assemblies on the proliferation and osteogenic gene expression of rat bone marrow stromal cells. *Biomaterials*. 2007; 28:1393–1403. [PubMed: 17166582]
66. Shelton RM, Liu Y, Cooper PR, Gbureck U, German MJ, Barralet JE. Bone marrow cell gene expression and tissue construct assembly using octacalcium phosphate microscaffolds. *Biomaterials*. 2006; 27:2874–2881. [PubMed: 16439012]
67. Suzuki O, Kamakura S, Katagiri T. Surface chemistry and biological responses to synthetic octacalcium phosphate. *J Biomed Mater Res B Appl Biomater*. 2006; 77:201–212. [PubMed: 16222696]

68. Miao X, Tan DM, Li J, Xiao Y, Crawford R. Mechanical and biological properties of hydroxyapatite/tricalcium phosphate scaffolds coated with poly(lactic-co-glycolic acid). *Acta Biomater.* 2008; 4:638–645. [PubMed: 18054297]
69. Dasgupta S, Tarafder S, Bandyopadhyay A, Bose S. Effect of grain size on mechanical, surface and biological properties of microwave sintered hydroxyapatite. *Mater Sci Eng C.* 2013; 33:2846–2854.
70. Rodriguez-Lorenzo LM, Vallet-Regi M, Ferreira JM, Ginebra MP, Aparicio C, Planell JA. Hydroxyapatite ceramic bodies with tailored mechanical properties for different applications. *J Biomed Mater Res.* 2002; 60:159–166. [PubMed: 11835171]
71. Ritchie RO. Mechanisms of fatigue crack propagation in ductile and brittle solids. *Int J Fract.* 1999; 100:55–83.
72. He F, Ye J. In vitro degradation, biocompatibility, and in vivo osteogenesis of poly(lactic-co-glycolic acid)/calcium phosphate cement scaffold with unidirectional lamellar pore structure. *J Biomed Mater Res A.* 2012; 100:3239–3250. [PubMed: 22733543]
73. Lu L, Garcia CA, Mikos AG. In vitro degradation of thin poly(DL-lactic-co-glycolic acid) films. *J Biomed Mater Res.* 1999; 46:236–244. [PubMed: 10380002]
74. van der Elst M, Klein CP, de Bleeck-Hogervorst JM, Patka P, Haarman HJ. Bone tissue response to biodegradable polymers used for intra medullary fracture fixation: A long-term in vivo study in sheep femora. *Biomaterials.* 1999; 20:121–128. [PubMed: 10022781]

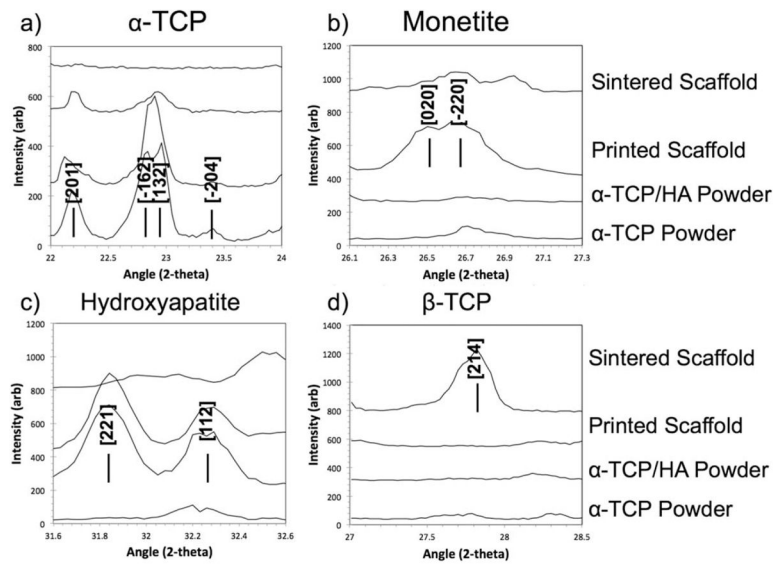
**FIGURE 1.**

Representative SEM images used to analyze powder particle diameter and distribution. (a)  $\alpha$ -TCP powder shows a polygonal morphology with an average diameter of  $56 \pm 27 \mu\text{m}$ . (b) HA powder shows a spherical morphology with an average diameter of  $27 \pm 10 \mu\text{m}$ . (c) PCL particles used for PCL codeposition showed polygonal morphology with an average particle diameter of  $256 \pm 100 \mu\text{m}$  ( $n = 4$  per material composition and aggregate data is shown in histograms). Bar =  $100 \mu\text{m}$  for all images.



**FIGURE 2.**

Representative XRD spectra of calcium phosphate phases of powders and 3D printed scaffolds. (a, b)  $\alpha$ -TCP and HA powder material demonstrates expected spectra for pure powder phases. (c) Monetite, a dicalcium phosphate phase, was shown to evolve using a 8.75% phosphoric acid printing solution. (d) Sintering at 1000°C for 6 h caused decomposition of  $\alpha$  phases to  $\beta$ -TCP ( $n=4$  per material composition).

**FIGURE 3.**

Representative XRD spectra of calcium phosphate phases of 3D printed scaffolds. (a)  $\alpha$ -TCP is partially consumed during printing, with conversion to monetite, then completely converted to  $\beta$ -TCP during sintering. (b) Evolution of monetite is observed following printing but is lost due to sintering. (c) HA is preserved during printing, however is lost due to sintering. (d)  $\beta$ -TCP evolves only following sintering ( $n=4$  per material composition).

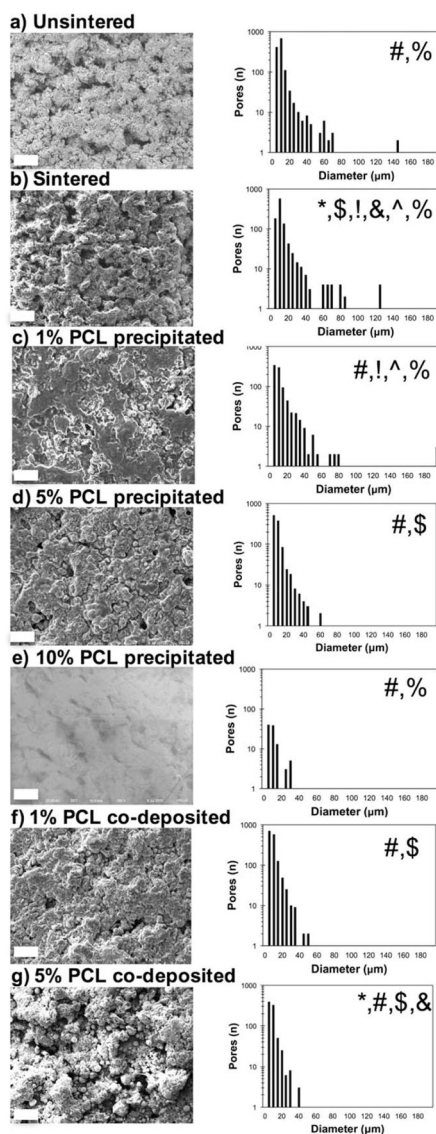


**FIGURE 4.**

Representative images used to analyze surface morphology of scaffolds with ImageJ thresholding and surface porosity measurements. (a) Unsintered, as-printed calcium phosphate scaffold. (b) Sintered (1000°C × 6 h) calcium phosphate scaffold. Calcium phosphate scaffold with (c) 1 wt % PCL precipitation (d) 5 wt % PCL precipitation and (e) 10 wt % PCL precipitation. Calcium phosphate scaffold with (f) 1 wt % (g) 5 wt % PCL codeposited. Data is average and standard deviation of five samples ( $n = 5$ ). Significance was evaluated using Kruskal–Wallis followed by Dunn’s analysis for multiple comparisons to compare as-printed scaffolds with treatments or within treatment groups with  $p < 0.05$  (multiplicity adjusted  $p$  values are listed in Table S1). \*, #, \$, !, ^, & denote significance compared to unsintered, sintered, 1 wt % PCL precipitation, 5 wt % PCL precipitation, 10 wt % PCL precipitation, 1 wt % PCL codeposition, and 5 wt % PCL codeposition, respectively. Bar = 100 µm for all.

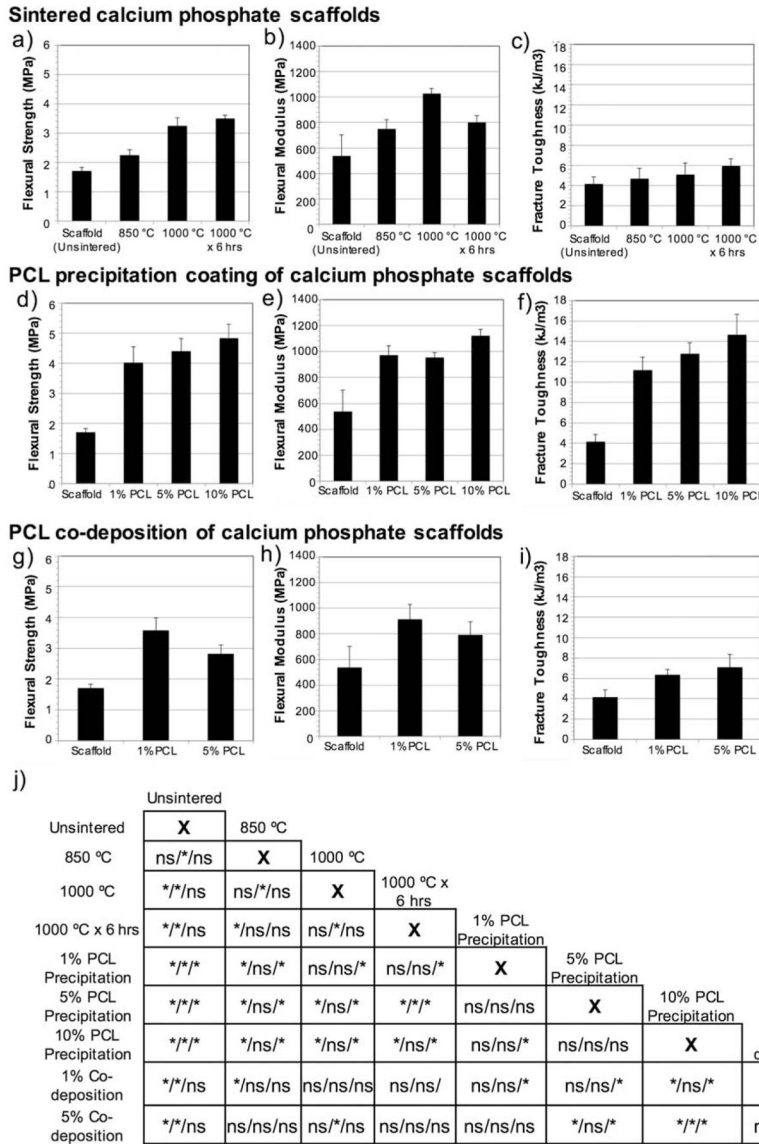


**FIGURE 5.** Mechanical properties of 3D printed CaP scaffolds analyzed through three-point bending. (a–c) Sintered calcium phosphate scaffolds, (d–f) PCL precipitated scaffolds, and (g–i) PCL codeposited scaffolds. Data are average and standard deviation of five samples ( $n = 5$ ). Significance was evaluated and shown in j using one-way ANOVA with Tukey’s test for multiple comparisons where \* indicates significance with  $p < 0.05$  for flexural strength, flexural modulus, and fracture toughness, respectively. ns, not significant. Multiplicity adjusted  $p$  values are reported in Table S2.